



# Transport coefficients of two-flavor superconducting quark matter

Mark G. Alford\*

*Physics Department, Washington University, St. Louis, Missouri 63130-4899, USA*

Hiroshi Nishimura†

*Faculty of Physics, University of Bielefeld, D-33615 Bielefeld, Germany*

Armen Sedrakian‡

*Institute for Theoretical Physics, J. W. Goethe-University, D-60438 Frankfurt am Main, Germany*

(Received 19 September 2014; published 13 November 2014)

**Background:** The two-flavor color superconducting (2SC) phase of quark matter is a possible constituent of the core of neutron stars. To assess its impact on the observable behavior of the star one must analyze transport properties, which in 2SC matter are controlled by the scattering of gapless fermionic modes by each other and possibly also by color-magnetic flux tubes.

**Purpose:** We determine the electrical and thermal conductivities and the shear viscosity of 2SC matter.

**Methods:** We use a variational formulation of transport theory, treating the strong and electromagnetic interactions via a weak coupling expansion.

**Results:** We provide the leading order scaling of the transport coefficients with temperature and chemical potential as well as accurate fits to our numerical results. We also find that the scattering of fermions by color-magnetic flux tubes is insignificant for thermal conductivity, but may contribute to the electrical conductivity and shear viscosity in the limit of very low temperature or high magnetic field. We also estimate the transport coefficients in unpaired quark matter.

**Conclusions:** Our calculation has set the stage for exploration of possible signatures of the presence of 2SC quark matter in neutron stars.

DOI: [10.1103/PhysRevC.90.055205](https://doi.org/10.1103/PhysRevC.90.055205)

PACS number(s): 97.60.Jd, 12.38.Mh, 47.32.C-, 67.10.Jn

## I. INTRODUCTION

Transport coefficients of dense matter play a central role in the modeling of astrophysical phenomena in compact stars. The thermal and magnetic evolution of compact stars, their rotational dynamics, and emission of electromagnetic and gravitational waves, all depend on the transport properties of different phases of dense matter.

In the core of a massive compact star, gravity compresses matter to a density where it may undergo a transition to quark matter which at sufficiently low temperature should be in one of the color superconducting phases [1,2]. Transport in a given phase is determined by the low-energy excitations of that phase, which are controlled by the symmetry breaking pattern. At asymptotically high density the favored phase is the color-flavor-locked (CFL) phase, where all the quark flavors and colors form Cooper pairs with zero total momentum [3]. The only excitations of the CFL phase at low temperature are superfluid phonons, whose interactions determine the transport coefficients of this phase [4–6]. The nature of quark pairing at lower densities, which may include the range relevant for compact stars, remains uncertain. One candidate is the two-flavor color-superconducting (2SC) phase, in which up ( $u$ ) quarks and down ( $d$ ) quarks pair in a color antitriplet state

leaving one of the colors unpaired [1,2]. In this paper we calculate key transport properties of this phase.

The paper is structured as follows. In Sec. II we discuss the relevant interactions among the ungapped fermions and calculate the scattering matrix elements for the fermions interacting via exchange of gauge bosons in the 2SC phase. Section III develops a general formalism for transport in multicomponent systems starting from the Boltzmann equation. After briefly explaining the physics of transport in the 2SC phase in Sec. IV A and our approximation schemes in Sec. IV B, we go on to compute the electrical conductivity, thermal conductivity, and shear viscosity of 2SC matter (Secs. IV C–IV E, respectively). In Sec. V we compare the fermion-fermion scattering contribution to the fermion-flux-tube scattering contribution and identify the domain where the latter could become important. Our results are summarized in Sec. VI. We use “Heaviside-Lorentz” natural units with  $\hbar = c = k_B = \epsilon_0 = 1$ , where  $k_B$  is the Boltzmann constant and  $\epsilon_0$  is the vacuum permittivity; the electric charge  $e$  is related to the fine structure constant by  $\alpha = e^2/(4\pi) = 1/137$  and similarly, the QCD coupling constant  $g$  by  $\alpha_s = g^2/(4\pi)$ .

## II. FERMION-FERMION SCATTERING IN THE 2SC PHASE

### A. Relevant excitations

The excitations that transport momentum and energy in 2SC superconductors are ungapped fermions. We fix to unitary gauge, where the 2SC condensate is uniform over all space

\*alford@wuphys.wustl.edu

†nishimura@physik.uni-bielefeld.de

‡sedrakian@th.physik.uni-frankfurt.de

and time, and use the standard convention that the condensate points in the red-green direction in color space. The red and green quarks, because of their 2SC pairing, have gaps  $\Delta$  which are expected to be around 10 MeV or larger [2,7] so their occupation is Boltzmann suppressed and they are frozen out of transport processes at temperatures appropriate to neutron stars. This leaves electrons and blue quarks as the only ungapped fermionic excitations. We will neglect muons and strange quarks. If they were present, their Fermi momenta and available phase space would be much smaller, so they would play a subleading role in transport processes. The main effect of strange quarks would be to reduce the electron population, affecting the dominance of electrons in transport.

The 2SC phase breaks no global symmetries, so there are no massless Goldstone bosons, or light pseudo-Goldstone bosons. The gauge bosons available to mediate fermion-fermion interactions in the 2SC phase are the eight gluons (generators  $T_A$ ) and the photon (generator  $Q$ ). However, because the transport coefficients are determined by the interactions only among the electron ( $e$ ), the blue up quark ( $bu$ ), and the blue down quark ( $bd$ ), most of the gauge bosons can be neglected. In the 2SC phase, the gauge symmetry breaking pattern is  $SU(3)_{\text{color}} \otimes U(1)_{\tilde{Q}} \rightarrow SU(2)_{rg} \otimes U(1)_{\tilde{Q}}$  [8,9]. The unbroken  $SU(2)_{rg}$  symmetry consists of color rotations involving the red and green colors. The unbroken  $U(1)_{\tilde{Q}}$  gauge symmetry is a linear combination of the original electromagnetic and color symmetries, called ‘‘rotated electromagnetism,’’ generated by  $\tilde{Q}$  which is a linear combination of  $Q$  and the eighth color generator  $T_8$ . The other linear combination of the gauge bosons is called the  $X$  boson, which is massive. The remaining gauge bosons are irrelevant because they do not couple to electrons, which have no color, and they cannot mediate interactions between blue quarks, because they all carry some nonblue color. As we will see, the transport properties of the 2SC phase are determined by the  $\tilde{Q}$  interaction, which is weakly coupled but long ranged (Landau damped), and the  $T_8$  and  $X$  interactions, which are strongly coupled but short ranged because of Debye and Meissner screening, respectively.

Lastly, we here compute the chemical potential of each flavor in the 2SC phase. The symmetry group of massless two-flavor QCD is  $SU(3)_{\text{color}} \times SU(2)_L \times SU(2)_R \times U(1)_B$ , where electromagnetism (generated by a combination of baryon number and isospin) and color are gauged. The relevant chemical potentials are  $\mu_q$  (coupled to quark number),  $\mu_e$  (coupled to negative electric charge), and  $\mu_3$  and  $\mu_8$  which are coupled to the Cartan generators of  $SU(3)_{\text{color}}$ ,  $T_3 = \text{diag}(1/2, -1/2, 0)$ , and  $T_8 = \text{diag}(1/(2\sqrt{3}), 1/(2\sqrt{3}), -1/\sqrt{3})$ . Because the color subgroup  $SU(2)_{rg}$ , which rotates red and green quarks, is unbroken in the 2SC phase, we have  $\mu_3 = 0$ . The chemical potentials for blue up and blue down quarks are, then,

$$\{\mu_{bu}, \mu_{bd}\} = \left\{ \mu_q - \frac{2}{3}\mu_e - \frac{1}{\sqrt{3}}\mu_8, \mu_q + \frac{1}{3}\mu_e - \frac{1}{\sqrt{3}}\mu_8 \right\}. \quad (1)$$

The rest of the quarks, red up ( $ru$ ), green up ( $gu$ ), red down ( $rd$ ), and green down ( $gd$ ), form the Cooper pairs, which have

average chemical potential,

$$\begin{aligned} \mu_C &= \frac{\mu_{ru} + \mu_{gd}}{2} = \frac{\mu_{gu} + \mu_{rd}}{2} \\ &= \mu_q - \frac{1}{6}\mu_e + \frac{1}{2\sqrt{3}}\mu_8. \end{aligned} \quad (2)$$

The Fermi surfaces of the paired fermion species are locked together with common Fermi momentum  $\mu_C$  [10]. The free energy density of 2SC quark matter without strange quarks is

$$\Omega_{2\text{SC}} = -\frac{\mu_{bu}^4}{12\pi^2} - \frac{\mu_{bd}^4}{12\pi^2} - \frac{\mu_e^4}{12\pi^2} - 4\frac{\mu_C^4}{12\pi^2} - \frac{\mu_C^2 \Delta^2}{\pi^2}. \quad (3)$$

The charge neutrality conditions,  $\partial\Omega_{2\text{SC}}/\partial\mu_e = 0$  and  $\partial\Omega_{2\text{SC}}/\partial\mu_8 = 0$ , are satisfied provided  $\mu_e = 3(2 + 3 \times 6^{1/3} - 6^{2/3})\mu_q/22$  and  $\mu_8 = \sqrt{3}(12 - 15 \times 6^{1/3} + 5 \times 6^{2/3})\mu_q/22$ , where we have ignored corrections of order  $\Delta^2/\mu_q^2$ . Thus each chemical potential in the 2SC phase is written in terms of the quark chemical potential  $\mu_q$  as

$$\{\mu_{bu}, \mu_{bd}, \mu_e, \mu_C\} \simeq \{0.566\mu_q, 1.13\mu_q, 0.566\mu_q, 0.934\mu_q\}. \quad (4)$$

To obtain a stable 2SC phase we require  $\Delta > \mu_e/2$  [11], but for  $\mu_e \gtrsim \Delta > \mu_e/2$  the terms of order  $\Delta^2/\mu_q^2$  that we have dropped only modify (4) by a few percent. We note that  $\mu_{bu} = \mu_e = \mu_{bd}/2$  even with the  $\Delta^2/\mu_q^2$  correction.

## B. Scattering matrix elements

Our analysis of transport in the 2SC phase of quark matter parallels that of Heiselberg and Pethick [12], who performed perturbative calculations for unpaired quark matter, assuming the strong coupling  $\alpha_s$  is small enough to make a perturbative expansion meaningful. We consider the scattering process of two incoming particles, particle 1 of type  $i$  and particle 2 of type  $j$ , into two outgoing particles, particle 3 of type  $i$  and particle 4 of type  $j$ . We denote four-momentum of particle  $n$  as  $(\epsilon_n, \mathbf{p}_n)$ , and  $\epsilon_n = |\mathbf{p}_n|$  because the Fermi momenta of the gapless fermions are large enough that we can neglect their masses. In the presence of scattering but no external force, the distribution function in momentum-position space of particle 1,  $f_1(\mathbf{x}, \mathbf{p}_1, t)$ , obeys the Boltzmann transport equation,

$$\begin{aligned} &\left( \frac{\partial}{\partial t} + \mathbf{v}_1 \cdot \nabla_{\mathbf{x}} \right) f_1 \\ &= -(2\pi)^4 \sum_j v_j \sum_{234} |M_{ij}|^2 [f_1 f_2 (1 - f_3)(1 - f_4) \\ &\quad - f_3 f_4 (1 - f_1)(1 - f_2)] \delta^4(p_{\text{in}} - p_{\text{out}}), \end{aligned} \quad (5)$$

where  $\sum_n = \int d^3 p_n / (2\pi)^3$ ,  $\delta^4(p_{\text{in}} - p_{\text{out}}) = \delta(\epsilon_{\text{in}} - \epsilon_{\text{out}}) \delta(\mathbf{p}_{\text{in}} - \mathbf{p}_{\text{out}})$ , and  $v_j = 2$  is the spin factor. The scattering matrix element  $M_{ij}$  is usually decomposed into longitudinal and transverse parts [13], and the longitudinal and transverse components of gauge boson self-energies in the static limit correspond to the Debye mass and the Meissner mass, respectively. According to [14,15], the Meissner mass matrix is diagonal in the rotated ( $X, \tilde{Q}$ ) basis, while the Debye

mass matrix is diagonal in the  $(T_8, Q)$  basis. Therefore, the two parts of the scattering matrix need to be expressed in the two different bases of the gauge bosons. We now show how to construct the scattering matrix below.

The indices  $i$  and  $j$  specify the species of the ungapped fermions, using the basis,

$$\begin{aligned} \Psi_i &= \{\Psi_{bu}, \Psi_{bd}, \Psi_e\} \\ &= \{\text{blue up quark } (bu), \text{ blue down quark } (bd), \\ &\quad \text{electron } (e)\}. \end{aligned} \quad (6)$$

The relevant gauge bosons can be written in either the  $(T_8, Q)$  or the  $(X, \tilde{Q})$  basis,

$$A_\mu = A_\mu^{T_8} T_8 + A_\mu^Q Q = A_\mu^X X + A_\mu^{\tilde{Q}} \tilde{Q}, \quad (7)$$

and we write the components as  $A_\mu^a$ , so  $a$  may vary over  $(T_8, Q)$  or  $(X, \tilde{Q})$  depending on the context. The components are related by

$$A_\mu^X = \cos \varphi A_\mu^{T_8} + \sin \varphi A_\mu^Q, \quad (8)$$

$$A_\mu^{\tilde{Q}} = -\sin \varphi A_\mu^{T_8} + \cos \varphi A_\mu^Q, \quad (9)$$

where the mixing angle  $\varphi$  is related to the QCD coupling  $g$  and the electromagnetic coupling  $e$  as [16]

$$\cos \varphi = \frac{\sqrt{3}g}{\sqrt{e^2 + 3g^2}}. \quad (10)$$

We write the covariant derivative as

$$D_\mu \Psi = \left( \partial_\mu - i \sum_a A_\mu^a Q^a \right) \Psi, \quad (11)$$

where  $Q^a$  is defined to be the product of the coupling constant and the charge matrix for the ungapped fermions:

$$\begin{aligned} Q^{T_8} &= g \times \text{diag} \left( -\frac{1}{\sqrt{3}}, -\frac{1}{\sqrt{3}}, 0 \right), \\ Q^Q &= e \times \text{diag} \left( +\frac{2}{3}, -\frac{1}{3}, -1 \right), \end{aligned} \quad (12)$$

in the  $(T_8, Q)$  basis and

$$\begin{aligned} Q^X &= g \cos \varphi \\ &\quad \times \text{diag} \left( -\frac{1 - 2 \tan^2 \varphi}{\sqrt{3}}, -\frac{1 + \tan^2 \varphi}{\sqrt{3}}, -\sqrt{3} \tan^2 \varphi \right), \\ Q^{\tilde{Q}} &= e \cos \varphi \times \text{diag}(1, 0, -1), \end{aligned} \quad (13)$$

in the  $(X, \tilde{Q})$  basis [16]. We will write the  $i$ th diagonal element as  $Q_i^a$ , defined by  $(Q^a)_{ij} = Q_i^a \delta_{ij}$  (with no sum over  $i$ ), and we give the values of  $Q_i^a$  in Table I.

Because of the screening in a plasma, the gauge bosons acquire self-energies  $\Pi_{\mu\nu}$ , which then contribute to the gauge field propagator,

$$(D_{\mu\nu}^{ab})^{-1} = g_{\mu\nu}(\omega^2 - q^2)\delta^{ab} + \Pi_{\mu\nu}^{ab}, \quad (14)$$

where  $\omega$  and  $\mathbf{q}$  are the energy and momentum transfer. We define  $q \equiv |\mathbf{q}|$  and similarly for other momenta. The scattering matrix element for two incoming particles, one with flavor  $i$

TABLE I. Value of  $Q_i^a$ , the product of the coupling constant and the charge, for each gauge boson  $a$  and each gapless fermion  $i$ . We also show the average for the two quarks in a Cooper pair.

	$Q^{T_8}$	$Q^Q$	$Q^X$	$Q^{\tilde{Q}}$
Blue up ( $bu$ )	$-g/\sqrt{3}$	$2e/3$	$-g \cos \varphi (1 - 2 \tan^2 \varphi)/\sqrt{3}$	$e \cos \varphi$
Blue down ( $bd$ )	$-g/\sqrt{3}$	$-e/3$	$-g \sec \varphi/\sqrt{3}$	0
Electron ( $e$ )	0	$-e$	$-\sqrt{3}g \sin \varphi \tan \varphi$	$-e \cos \varphi$
Cooper pair ( $C$ )	$g/(2\sqrt{3})$	$e/6$	$g \sec \varphi/(2\sqrt{3})$	0

and four-momentum  $(\epsilon_1, \mathbf{p}_1)$  and the other with flavor  $j$  and four-momentum  $(\epsilon_2, \mathbf{p}_2)$ , is

$$M_{ij} = J_{a,i}^\mu (D_{\mu\nu}^{ab}) J_{b,j}^\nu, \quad (15)$$

$$J_{a,i}^\mu = Q_i^a \bar{u}(\mathbf{p}_3) \gamma^\mu u(\mathbf{p}_1) / 2p_1, \quad (16)$$

$$J_{b,j}^\nu = Q_j^b \bar{u}(\mathbf{p}_4) \gamma^\nu u(\mathbf{p}_2) / 2p_2, \quad (17)$$

where  $J_{a,i}^\mu$  and  $J_{b,j}^\nu$  are the transition currents,  $\gamma^\mu$  is a Dirac matrix, and  $u$  is the Dirac spinor.

We split the current into the longitudinal component,  $J^l = \mathbf{J} \cdot \hat{\mathbf{q}} = \omega J^0 / q$ , and the transverse component,  $\mathbf{J}^t = \mathbf{J} - J^l \hat{\mathbf{q}}$ . We denote the corresponding self-energies in the propagator as  $\Pi_l^{ab}$  and  $\Pi_t^{ab}$ , respectively. Because the longitudinal components of the propagator are diagonal in the  $(T_8, Q)$  basis and the transverse components are diagonal in the  $(X, \tilde{Q})$  basis [14,15], we can write the matrix element as

$$M_{ij} = \sum_{a=\{T_8, Q\}} \frac{J_{a,i}^0 J_{a,j}^0}{q^2 + \Pi_l^{aa}} - \sum_{a=\{X, \tilde{Q}\}} \frac{\mathbf{J}_{a,i}^t \cdot \mathbf{J}_{a,j}^t}{q^2 - \omega^2 + \Pi_t^{aa}}, \quad (18)$$

and after summing over the final spins and averaging over the initial spins, the scattering matrix element can be written as

$$\begin{aligned} |M_{ij}|^2 &= L_l \left| \sum_{a=\{T_8, Q\}} \frac{Q_i^a Q_j^a}{q^2 + \Pi_l^{aa}} \right|^2 \\ &\quad + L_t \left| \sum_{a=\{X, \tilde{Q}\}} \frac{Q_i^a Q_j^a}{q^2 - \omega^2 + \Pi_t^{aa}} \right|^2 \\ &\quad - 2L_{lt} \text{Re} \left[ \left( \sum_{a=\{T_8, Q\}} \frac{Q_i^a Q_j^a}{q^2 + \Pi_l^{aa}} \right) \right. \\ &\quad \left. \times \left( \sum_{a=\{X, \tilde{Q}\}} \frac{Q_i^a Q_j^a}{q^2 - \omega^2 + \Pi_t^{aa}} \right)^* \right] + \delta_{ij} \gamma_{\text{int}}, \end{aligned} \quad (19)$$

where  $\gamma_{\text{int}}$  is the interference term, which is the cross term of two different channels for two identical incoming particles. As discussed in [17], however, it is small in the weak-screening approximation, so we neglect  $\gamma_{\text{int}}$ . In the limit  $\omega \ll p, \mu_q, L^s$

become

$$\begin{aligned} L_l &= \left(1 - \frac{q^2}{4p_1^2}\right) \left(1 - \frac{q^2}{4p_2^2}\right), & L_{ll} &= \left(1 - \frac{q^2}{4p_1^2}\right)^{1/2} \left(1 - \frac{q^2}{4p_2^2}\right)^{1/2} \cos \theta, \\ L_t &= \left(1 - \frac{q^2}{4p_1^2}\right) \left(1 - \frac{q^2}{4p_2^2}\right) \cos^2 \theta + \frac{q^2}{4p_1^2} + \frac{q^2}{4p_2^2}, \end{aligned} \quad (20)$$

where  $\theta$  is the angle between  $\mathbf{p}_1 + \mathbf{p}_3$  and  $\mathbf{p}_2 + \mathbf{p}_4$  [17].

The one-loop correction of self-energies comes from the ungapped fermions and the Cooper pairs. Following Appendix A in [18], we parametrize the longitudinal component  $\Pi_l$  and transverse component  $\Pi_t$  as

$$\begin{aligned} \Pi_l^{aa} &= \sum_i (q_{D,i}^a)^2 \chi_l + 4(q_{D,C}^a)^2 \chi_l && \text{in the } (T_8, Q) \text{ basis,} \\ \Pi_t^{aa} &= \sum_i (q_{D,i}^a)^2 \chi_t + 4(q_{D,C}^a)^2 \chi_t + 4(q_{D,C}^a)^2 \chi_{sc} && \text{in the } (X, \tilde{Q}) \text{ basis,} \end{aligned} \quad (21)$$

where  $q_{D,i}^a$  and  $q_{D,C}^a$  are the Debye masses for a given flavor  $i$  and the Cooper pair, respectively, and the factors of 4 in front of  $(q_{D,C}^a)^2$  arise from the four different species of Cooper pairs in the 2SC phase. The Debye masses are

$$(q_{D,i}^a)^2 = (Q_i^a)^2 \frac{\mu_i^2}{\pi^2}, \quad (22)$$

$$(q_{D,C}^a)^2 = (Q_C^a)^2 \frac{\mu_C^2}{\pi^2}, \quad (23)$$

where  $\mu_i$  and  $\mu_C$  are the chemical potentials of fermion with flavor  $i$  and the Cooper pair, respectively.  $Q_C^a$  is a product of a coupling constant and the average charge of the two quarks that constitute the pair [19] (see Table I). The Cooper pair has  $X$  charge but no  $\tilde{Q}$  charge, so in the static limit where  $\omega/q \ll 1$ ,  $\Pi_t^{XX}$  has a real component, which gives the Meissner effect, while  $\Pi_t^{\tilde{Q}\tilde{Q}}$  has an imaginary component, which gives the Landau damping. The screening functions,  $\chi_l$  and  $\chi_t$ , are functions of  $\omega$  and  $q$ , and are calculated in [20–22]. In this paper, we use the static limit of the screening functions [12,19],

$$\chi_l = 1, \quad \chi_t = i \frac{\pi}{4} \frac{\omega}{q}, \quad \chi_{sc} = \frac{1}{3}. \quad (24)$$

Taking the leading order in  $\omega/q$ , we thus have

$$\Pi_l^{T_8 T_8} = \sum_i (Q_i^{T_8})^2 \frac{\mu_i^2}{\pi^2} + 4(Q_C^{T_8})^2 \frac{\mu_C^2}{\pi^2}, \quad (25)$$

$$\Pi_t^{Q Q} = \sum_i (Q_i^Q)^2 \frac{\mu_i^2}{\pi^2} + 4(Q_C^Q)^2 \frac{\mu_C^2}{\pi^2}, \quad (26)$$

$$\Pi_t^{X X} = \frac{4}{3} (Q_C^X)^2 \frac{\mu_C^2}{\pi^2}, \quad (27)$$

$$\Pi_t^{\tilde{Q}\tilde{Q}} = i \frac{\omega}{q} \Lambda^2 \quad \text{where} \quad \Lambda^2 \equiv \sum_i (Q_i^{\tilde{Q}})^2 \frac{\mu_i^2}{4\pi}, \quad (28)$$

where  $Q$ 's are given in Table I.

### III. TRANSPORT COEFFICIENTS IN A MULTICOMPONENT SYSTEM

In preparation for our calculation of the transport properties of the 2SC phase, we write down transport coefficients in

a general multicomponent system at low temperature and high density,  $T/\mu \ll 1$ , using the linear Boltzmann transport equation in the relaxation time approximation. We consider an isotropic system which is weakly perturbed from its equilibrium state. In this case, the electrical conductivity  $\sigma$ , the thermal conductivity  $\kappa$ , and the shear viscosity  $\eta$ , are related to the electric current  $j_\alpha$ , the heat flux  $h_\alpha$ , and the shear stress tensor  $\sigma_{\alpha\beta}$ , respectively, as [23]

$$j_\alpha = -\sigma \partial_\alpha U, \quad (29)$$

$$h_\alpha = -\kappa \partial_\alpha T, \quad (30)$$

$$\sigma_{\alpha\beta} = -\eta V_{\alpha\beta}, \quad (31)$$

where  $U$  is the electric potential and  $V_{\alpha\beta}$  is the traceless part of the spatial derivative of fluid velocity  $\mathbf{V}$ ,

$$V_{\alpha\beta} = \partial_\alpha V_\beta + \partial_\beta V_\alpha - \frac{2}{3} \delta_{\alpha\beta} \nabla \cdot \mathbf{V}. \quad (32)$$

We use  $\alpha, \beta, \lambda,$  and  $\rho$  as spatial indices. From kinetic theory, we can write the fluxes on the left-hand sides as [24]

$$j_\alpha = \int \frac{d^3 p}{(2\pi)^3} e v_\alpha \delta f, \quad (33)$$

$$h_\alpha = \int \frac{d^3 p}{(2\pi)^3} (\epsilon - \mu) v_\alpha \delta f, \quad (34)$$

$$\sigma_{\alpha\beta} = \int \frac{d^3 p}{(2\pi)^3} p_\alpha v_\beta \delta f, \quad (35)$$

where  $v_\alpha$  is the particle velocity with  $|v_\alpha| = 1$ , and  $\delta f$  is a deviation from the equilibrium distribution function  $f^0$ . As we explained in the previous section, the fermions that contribute to the transport properties in the 2SC phase are the blue up quark, blue down quark, and electron. In general, we can combine the above equations to write for a multicomponent system as [25–27]

$$\xi Y = \sum_i v_i \int \frac{d^3 p}{(2\pi)^3} \phi_i \delta f_i, \quad (36)$$

where  $v_i$  is a spin factor for a particle flavor  $i$ . Instead of writing three different equations for the transport coefficients, we have defined  $\xi$  as a transport coefficient for  $\sigma, \kappa,$  or  $\eta$  with corresponding macroscopic quantity  $Y$  ( $-\partial_\alpha U, -\partial_\alpha T,$  or

$-V_{\alpha\beta}$ , respectively) and a microscopic quantity,

$$\phi_i = \begin{cases} e_i v_\alpha & \text{Electrical conductivity} \\ (\epsilon - \mu_i) v_\alpha & \text{Thermal conductivity} \\ p_\alpha v_\beta & \text{Shear viscosity} \end{cases}, \quad (37)$$

respectively. We treat  $Y$  and  $\phi_i$  as matrices for the shear viscosity and vectors for the thermal and electrical conductivities. We write each distribution function with flavor  $i$  as

$$f_i = f_i^0 + \delta f_i = \frac{1}{e^{(\epsilon - \mu_i)/T} + 1} - \frac{\partial f_i^0}{\partial \epsilon} \Phi_i, \quad (38)$$

and we further parametrize the unknown coefficient  $\Phi_i$  using the relaxation time approximation [17,28]:

$$\Phi_i = 3\tau_i \psi_i \cdot Y, \quad (39)$$

where  $\tau_i$  is a relaxation time.  $\psi_i \cdot Y$  denotes the dot product for vectors and the Hadamard product for matrices, i.e.,  $\psi_i \cdot Y \equiv (\psi_i)_{\alpha\beta} Y^{\alpha\beta}$ . The numerical factor of 3 is given so that the definition of the relaxation time agrees with that of Heiselberg and Pethick [12].  $\psi_i$  is a microscopic quantity

$$Y = \begin{cases} -\partial_\alpha U = -\delta_\alpha^\lambda \partial_\lambda U & \text{Electrical conductivity} \\ -\partial_\alpha T = -\delta_\alpha^\lambda \partial_\lambda T & \text{Thermal conductivity} \\ -V_{\alpha\beta} = -\frac{1}{2} \left( \delta_\alpha^\lambda \delta_\beta^\rho + \delta_\alpha^\rho \delta_\beta^\lambda - \frac{2}{3} \delta_{\alpha\beta} \delta^{\lambda\rho} \right) V_{\lambda\rho} & \text{Shear viscosity} \end{cases}, \quad (43)$$

and then we can divide the common factor of  $Y$  on both sides in Eq. (42) and contract the indices  $\alpha$  and  $\lambda$  for the electrical and thermal conductivities and the pairs of indices  $\alpha, \lambda$  and  $\beta, \rho$  for the shear viscosity. This gives us an expression for a generic transport coefficient,

$$\xi_i = -\frac{3\tau_i v_i}{\gamma} \int \frac{d^3 p}{(2\pi)^3} (\phi_i \cdot \psi_i) \frac{\partial f_i^0}{\partial \epsilon}, \quad (44)$$

where  $\gamma$  is a numerical factor after contracting the indices:  $\gamma = \delta_\alpha^\alpha = 3$  for the electrical and thermal conductivities and  $\gamma = (\delta_\alpha^\alpha \delta_\beta^\beta + \delta_\alpha^\alpha - 2\delta_\alpha^\alpha/3)/2 = 5$  for the shear viscosity.

From the Boltzmann equation, we can obtain another expression for a transport coefficient. By taking the leading order in the derivative expansion of the Boltzmann transport equation, Eq. (5), we obtain the linearized Boltzmann equation:

$$\begin{aligned} \psi_i \cdot Y \frac{\partial f_i^0}{\partial \epsilon_1} &= -\frac{(2\pi)^4}{T} \sum_j v_j \sum_{234} |M_{ij}|^2 f_1^0 f_2^0 (1 - f_3^0) (1 - f_4^0) \\ &\times \delta^4(p_{\text{in}} - p_{\text{out}}) (\Phi_1 + \Phi_2 - \Phi_3 - \Phi_4). \end{aligned} \quad (45)$$

depending on the transport phenomena, and the standard forms<sup>1</sup> are given as [24]

$$\psi_i = \begin{cases} e_i v_\alpha & \text{Electrical conductivity} \\ (\epsilon - \mu_i) v_\alpha / T & \text{Thermal conductivity} \\ (p_\alpha v_\beta - \frac{1}{3} \delta_{\alpha\beta} \mathbf{p} \cdot \mathbf{v}) / 2 & \text{Shear viscosity} \end{cases}. \quad (40)$$

From Eq. (36), we can now define transport coefficient of each component  $\xi_i$  as

$$\xi = \sum_i \xi_i = \xi_{bu} + \xi_{bd} + \xi_e, \quad (41)$$

with

$$\xi_i Y = -3\tau_i v_i \int \frac{d^3 p}{(2\pi)^3} \phi_i (\psi_i \cdot Y) \frac{\partial f_i^0}{\partial \epsilon}. \quad (42)$$

Following the standard procedure, we rewrite  $Y$  as

Acting with  $-3\tau_i v_i \sum_1 \phi_1$  on both sides, we obtain

$$\begin{aligned} \xi_i Y &= 3\tau_i \frac{(2\pi)^4}{T} \sum_j v_i v_j \sum_{1234} |M_{ij}|^2 f_1^0 f_2^0 (1 - f_3^0) (1 - f_4^0) \\ &\times \delta^4(p_{\text{in}} - p_{\text{out}}) \phi_1 [3\tau_i (\psi_1 - \psi_3) + 3\tau_j (\psi_2 - \psi_4)] \cdot Y, \end{aligned} \quad (46)$$

and using the same procedure that led us to Eq. (44), we have

$$\begin{aligned} \xi_i &= \frac{9\tau_i (2\pi)^4}{\gamma T} \sum_j v_i v_j \sum_{1234} |M_{ij}|^2 f_1^0 f_2^0 (1 - f_3^0) (1 - f_4^0) \\ &\times \delta^4(p_{\text{in}} - p_{\text{out}}) \phi_1 \cdot [\tau_i (\psi_1 - \psi_3) + \tau_j (\psi_2 - \psi_4)]. \end{aligned} \quad (47)$$

After taking the limit  $\omega, T \ll \mu_q$  [12], we finally have

$$\begin{aligned} \xi_i &= \frac{\tau_i}{\gamma} \sum_j v_i v_j \frac{36T \mu_i^2 \mu_j^2}{(2\pi)^5} \int_0^\infty d\omega \left( \frac{\omega/2T}{\sinh(\omega/2T)} \right)^2 \\ &\times \int_0^{q_M} dq \int_0^{2\pi} \frac{d\theta}{2\pi} |M_{ij}|^2 \phi_1 \\ &\cdot [\tau_i (\psi_1 - \psi_3) + \tau_j (\psi_2 - \psi_4)], \end{aligned} \quad (48)$$

where  $q_M = \min[2p_1, 2p_2] = \min[2\mu_i, 2\mu_j]$  is the maximum momentum transfer, and  $\theta$  is again the angle between  $\mathbf{p}_1 + \mathbf{p}_3$  and  $\mathbf{p}_2 + \mathbf{p}_4$ . The momentum of an incoming fermion is the Fermi momentum in the limit  $T/\mu_q \ll 1$ , so we simply replace all  $p_1$  and  $p_2$  with  $\mu_i$  and  $\mu_j$ , respectively. Equations (44) and (48) can be used to find the relaxation times  $\tau_i$  for the three gapless fermion species, and thus their contributions  $\xi_i$  to the transport coefficient.

<sup>1</sup>We could use the Chapman-Enskog method and write each  $\psi_i$  as an infinite sum of trial functions, but one trial function with correct power of momentum is usually sufficient. See, e.g., [29,30].



#### IV. TRANSPORT PROPERTIES IN THE 2SC PHASE

##### A. The physics of transport in 2SC quark matter

Transport in the 2SC phase occurs via the ungapped fermions: the blue up quark, the blue down quark, and the electron. At a given temperature, transport is dominated by the fermion that feels the least influence from the surrounding particles because it will have a long relaxation time or mean free path. The relevant interactions (and their generators) are as follows. The longitudinal strong interaction ( $T_8$ ) and the longitudinal electromagnetic interaction ( $Q$ ), which are both short ranged because of Debye screening; the transverse “rotated” strong interaction ( $X$ ) which is short ranged because of Meissner screening; and the transverse “rotated” electromagnetic interaction ( $\tilde{Q}$ ), which is not screened, only Landau damped.

At low temperatures, where the typical energy transfer  $\omega$  is small, Landau damping [which is proportional to  $\omega$  (28)] becomes a small effect, making the  $\tilde{Q}$  interaction long ranged. The  $bu$  quark and electron, which carry  $\tilde{Q}$  charge, therefore experience more scattering than the  $bd$  quark, whose  $\tilde{Q}$  charge is zero, so their relaxation time is short and transport is dominated by the  $bd$  quark. The essential point is that at low temperature the long range of the  $\tilde{Q}$  interaction compensates for its small inherent coupling, so particles that feel the  $\tilde{Q}$  interaction have suppressed contributions to transport.

At high temperatures, where typical energy transfers are large, the Landau damping of the  $\tilde{Q}$  becomes more significant, and it no longer has such a long range. Relaxation times are then determined by the strong interaction ( $T_8$  and  $X$ ), so the electron, which has no  $T_8$  charge and only a very small  $X$  charge, dominates transport. The next most important fermion is the blue down quark, simply because its Fermi momentum is larger (4), so there are more states near its Fermi surface.

We therefore expect that as temperature rises, we start off in a regime dominated by the  $bd$  quark, and then make a transition to a regime dominated by electrons. As we will see, this transition occurs at different temperatures for different transport properties.

##### B. Approximation schemes

We now compute the electrical conductivity, the thermal conductivity, and the shear viscosity in the 2SC phase using the formalism developed in Sec. III. In each case we perform a numerical calculation and obtain an analytic approximation to it. The coefficients will be functions of two parameters of microscopic physics, the strong coupling  $\alpha_s$  and electromagnetic coupling  $\alpha$ , and two thermodynamic potentials, the quark chemical potential  $\mu_q$  and the temperature  $T$ . Following Heiselberg and Pethick [12], we will calculate to leading order in  $\alpha_s$  and, for quantities dominated by electromagnetism, in  $\alpha$ . This gives results that are reliable at very high energy scales, but provides at best a rough estimate of the values of the transport coefficients at the energy scales relevant for compact star phenomenology because the strong interaction is nonperturbative in that regime. For numerical estimates we will take  $\alpha_s = 1$ .

The relevant temperature range for compact star phenomenology is from about 10 keV to 1 MeV while the

density regime of interest requires quark chemical potential  $\mu_q \sim 400$  MeV. We will therefore make use of an expansion in powers of  $T/\mu_q$ . For numerical computations, we present results for  $T/\mu_q$  in the range from  $10^{-5}$  to  $10^{-3}$ . We can assume that the energy transfer is much smaller than the momentum transfer,  $\omega \ll q$ , because the characteristic energy transfer is of the order of the temperature ( $\omega \sim T$ ), and the characteristic momentum transfer is roughly the screening scale (of order  $e\mu$  or  $g\mu$ ) of the relevant gauge bosons. Terms such as  $q^2 - \omega^2 + \Pi_i^{aa}$  in the transverse component of the scattering matrix element in Eq. (19) become  $q^2 + \Pi_i^{aa}$ .

For physical insight we will also obtain analytic approximations by using the additional simplifying assumption that the momentum transfer is much smaller than the quark chemical potential,  $q \ll \mu_q$ . This is a good approximation for the transverse component of the  $\tilde{Q}$  interaction [17], because the self-energy of the  $\tilde{Q}$  boson is Landau damped, and the characteristic momentum transfer is  $q \sim (e^2\mu_q^2 T)^{1/3} \ll \mu_q$ . Therefore, even for the numerical computations, we use the analytical expression for the  $\tilde{Q}$  interaction [third lines of Eqs. (54) and (62)] by taking the limit  $q \ll \mu_q$  in Eq. (48). As pointed out by Shternin and Yakovlev [17], the approximation is not always reliable for screened interactions: High momentum transfer processes sometimes play an important role. However, we will show that these analytic results agree well with the numerical results in the 2SC phase, and they provide us with a physical understanding of the numerical results.

##### C. Electrical conductivity of $\tilde{Q}$ charge

In the 2SC phase, electrical conductivity involves  $\tilde{Q}$  charge rather than  $Q$  charge. A charged current produces magnetic fields, but  $X$  magnetic fields are Meissner screened, so only the  $\tilde{Q}$  current exists in the bulk of 2SC matter. The expected behavior discussed in Sec. IV A is affected by the fact that  $bd$  quarks have no  $\tilde{Q}$  charge, so their low-temperature dominance of transport is not relevant to electrical conductivity.  $\tilde{Q}$  charge is carried by the electron and the blue up quark, which have  $\tilde{Q}$  interactions with each other. However, the blue up quark has a shorter relaxation time because of its additional strong interactions with the blue down quarks, so conductivity will be dominated by the electron. We will see below how our calculations confirm this expectation.

For the electrical conductivity of  $\tilde{Q}$  charge, we have  $\phi_i = Q_i^{\tilde{Q}} v_\alpha$  and  $\gamma = 3$  in Eq. (44), which then gives the Drude result for the conductivity of species  $i$  with relaxation time  $\tau_i^\sigma$ ,

$$\sigma_i = \tau_i^\sigma \frac{\mu_i^2 (Q_i^{\tilde{Q}})^2}{\pi^2}. \quad (49)$$

Because  $Q_{bd}^{\tilde{Q}}$  is zero,  $\sigma_{bd} = 0$ . To calculate  $\tau_i^\sigma$  using Eq. (48), we write

$$\begin{aligned} & \phi_1 \cdot [\tau_i^\sigma (\psi_1 - \psi_3) + \tau_j^\sigma (\psi_2 - \psi_4)] \\ &= \frac{(Q_i^{\tilde{Q}})^2}{2p_1^2} \left( \tau_i^\sigma - \tau_j^\sigma \frac{p_1 Q_j^{\tilde{Q}}}{p_2 Q_i^{\tilde{Q}}} \right) q^2, \end{aligned} \quad (50)$$

where we have ignored the terms suppressed by factors of  $\omega/p_{1,2}$ . Using the above two equations in Eq. (48),

we find

$$1 = \frac{3T}{4\pi^3} \sum_j \frac{\mu_j^2}{\mu_i^2} \left( \tau_i^\sigma - \tau_j^\sigma \frac{\mu_i Q_j^{\tilde{Q}}}{\mu_j Q_i^{\tilde{Q}}} \right) s_{ij}^\sigma, \quad (51)$$

for a flavor  $i = bu$  or  $e$ , where

$$s_{ij}^\sigma = \int_0^\infty d\omega \left( \frac{\omega/2T}{\sinh(\omega/2T)} \right)^2 \int_0^{q_M} dq \int_0^{2\pi} \frac{d\theta}{2\pi} |M_{ij}|^2 q^2, \quad (52)$$

which is symmetric in exchanging  $i$  and  $j$ . We can then solve Eq. (51) for the relaxation times,  $\tau_{bu}^\sigma$  and  $\tau_e^\sigma$ , and find

$$\frac{1}{\tau_i^\sigma} = \frac{3T}{4\pi^3} s_{i,bd}^\sigma s_{bu,e}^\sigma \left( \frac{1}{s_{bu,bd}^\sigma} + \frac{4}{s_{bu,e}^\sigma} + \frac{1}{s_{bd,e}^\sigma} \right), \quad (53)$$

where  $i = bu$  or  $e$ . Even though  $\sigma_{bd} = 0$ , the blue down quark has some effect on the conductivity because its interactions with the charged fermions, particularly the  $bu$  quark, affect their relaxation rates. We numerically integrate Eq. (52) using the scattering matrix element  $M_{ij}$  given in Eq. (19), with the charges from Table I with  $\alpha = 1/137$  and  $\alpha_s = 1$ ,  $L$ 's from Eq. (20) with  $p_1 = \mu_i$  and  $p_2 = \mu_j$ , the boson self-energies from Eqs. (25)–(28), and the chemical potentials from Eq. (4).  $s^\sigma$  is then a dimensionless function of  $T/\mu_q$ . We use the numerical value of  $s^\sigma$  in Eq. (53) to obtain  $\tau_i^\sigma \mu_q$ , which then gives  $\sigma_i/\mu_q$  by Eq. (49). The results are plotted in Fig. 1, and the best fits are  $\sigma_{bu}/\mu_q = 0.000672/((T/\mu_q)^{5/3} + 2.11(T/\mu_q)^2)$  and  $\sigma_e/\mu_q = 1.46/((T/\mu_q)^{5/3} + 2.11(T/\mu_q)^2)$ . We note these fits can be extrapolated to arbitrary low temperature.

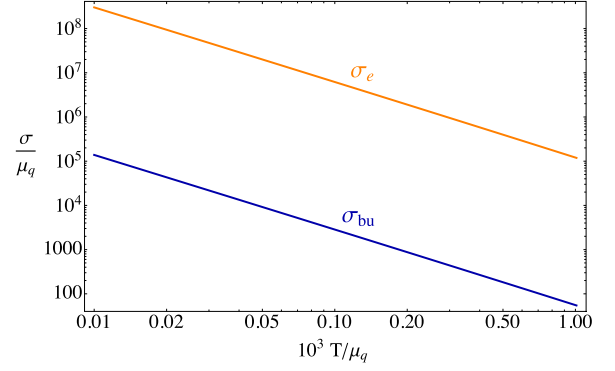


FIG. 1. (Color online) Numerically calculated electrical ( $\tilde{Q}$ ) conductivity as a function of temperature, both expressed in units of the quark chemical potential  $\mu_q$ , taking strong interaction coupling  $\alpha_s = 1$ . The electrons dominate because the  $bu$  relaxation time is shortened by its strong interaction with the  $bd$  quarks.

We see in Fig. 1 that the electrons dominate the conductivity, obeying a  $T^{-5/3}$  power law. To understand this we now derive an approximate analytic expression for the electrical conductivity by assuming that the momentum transfer  $q$  is much less than the typical Fermi momenta. In this limit,  $q \ll \mu_q \sim p_{1,2}$ , Eq. (20) simply becomes  $L_l = 1$ ,  $L_{lt} = \cos\theta$ , and  $L_t = \cos^2\theta$ . Furthermore, the upper interval of the  $q$  integral in Eq. (52) may be taken as infinity because the integrand is very small for  $q \gtrsim q_M$ . The integral in Eq. (52) can then be performed analytically [12] using the identity,

$$\int_0^\infty d\omega \left( \frac{\omega/2T}{\sinh(\omega/2T)} \right)^2 \int_0^\infty dq \operatorname{Re} \left[ \frac{q^2}{(q^2 + \Pi^{aa})(q^2 + \Pi^{bb})^*} \right] = \begin{cases} \frac{\pi^3 T}{6(\sqrt{\Pi^{aa}} + \sqrt{\Pi^{bb}})} & \text{if neither } a \text{ nor } b \text{ is } \tilde{Q} \\ \frac{\pi^3 T}{6\sqrt{\Pi^{aa}}} + \mathcal{O}\left(\frac{T^{4/3}}{\mu_q}\right) & \text{if } b \text{ is } \tilde{Q} \text{ and } a \text{ is not } \\ \frac{\pi\Gamma(8/3)\zeta(5/3)T^{2/3}}{3\Lambda^{2/3}} & \text{if } a \text{ and } b \text{ are both } \tilde{Q} \end{cases}, \quad (54)$$

where  $\Pi^{aa}$  is a self-energy of a boson of type  $a$ , with the convention that  $\Pi^{aa} = \Pi_l^{aa}$  if  $a$  is either  $T_8$  or  $Q$  and  $\Pi^{aa} = \Pi_t^{aa}$  if  $a$  is either  $X$  or  $\tilde{Q}$ , as given in Eqs. (25)–(28). For the first case, both the gauge boson self-energies  $\Pi^{aa}$  and  $\Pi^{bb}$  are independent of  $\omega$  and  $q$ , so the integration can be performed straightforwardly. In the second case, one of the self-energies is for the  $\tilde{Q}$  photon, which is dominated by Landau damping,  $\Pi_t^{\tilde{Q}\tilde{Q}} = i\omega\Lambda^2/q$  (28). In this case, we first perform the  $q$  integral exactly, then keep the leading order in  $\omega/\mu_q$  because  $\omega \sim T \ll \mu_q$ , and finally perform the  $\omega$  integral exactly. This is equivalent to doing the integral exactly by neglecting  $\Pi_t^{\tilde{Q}\tilde{Q}}$  because  $\omega/q \ll 1$ . In the third case, however, both the self-energies are for  $\tilde{Q}$  photons; their Landau damping acts as the regulator of an infrared divergence and the integral scales as  $(T/\Lambda)^{2/3}$ . We call this the “ $\tilde{Q}$ -interaction term.” We thus find

$$s_{ij}^\sigma = \frac{\pi^3 T}{6} \sum_{a,b=(T_8,Q)} \frac{Q_i^a Q_j^a Q_i^b Q_j^b}{\sqrt{\Pi_l^{aa}} + \sqrt{\Pi_l^{bb}}} + \frac{\pi^3 T}{12} \left( \frac{(Q_i^X)^2 (Q_j^X)^2}{2\sqrt{\Pi_t^{XX}}} + \frac{2Q_i^X Q_j^X Q_i^{\tilde{Q}} Q_j^{\tilde{Q}}}{\sqrt{\Pi_t^{XX}}} \right) + \frac{\pi\Gamma(8/3)\zeta(5/3)T^{2/3}}{6} \frac{(Q_i^{\tilde{Q}})^2 (Q_j^{\tilde{Q}})^2}{\Lambda^{2/3}}, \quad (55)$$

where the self-energies are given in Eqs. (25)–(28). The first term comes from the longitudinal interactions and the rest comes from the transverse interactions. As shown in [12], the  $\tilde{Q}$ -interaction term has a lower power of the temperature because Landau damping gives a small contribution to the self-energy at low energy transfer, making the  $\tilde{Q}$  interaction long ranged at low temperature. If we use this analytic approximation in Eqs. (53) and (49), then we obtain values of  $\tau_{bu}^\sigma$  and  $\tau_e^\sigma$  that agree with the numerical evaluation to within 35% and 4%, respectively, at temperatures up to  $10^{-3}\mu_q$ .

We can explain qualitatively why  $\sigma_e$  is much larger than  $\sigma_{bu}$ . From Eqs. (49) and (53), we have  $\sigma_e/\sigma_{bu} = \tau_e/\tau_{bu} = s_{bu,bd}^\sigma/s_{e,bd}^\sigma$  where the first equality comes from the fact that the blue up quark and the electron have the same chemical potential and the opposite  $\tilde{Q}$  charge. From Eq. (55), we find that  $s_{bu,bd}^\sigma$  is proportional to  $g^3$  because the main interactions are the screened strong interactions by the  $T_8$  and  $X$  bosons.  $s_{bd,e}^\sigma$  is proportional to  $e^3$  because it is dominated by the longitudinal screened electromagnetic  $Q$  interaction. Thus we can estimate that  $\sigma_e/\sigma_{bu} \sim (g/e)^3 \sim 10^3$ , which qualitatively agrees with Fig. 1.

We now explicitly show the analytical expression for the dominant contribution of  $\sigma_e$ . The first term in Eq. (53) is negligible compared to the other two terms because  $s_{bu,bd}^\sigma$  is proportional to a scattering amplitude of the strong interaction. Thus we have

$$\frac{1}{\tau_e^\sigma} = \frac{3T}{4\pi^3} (4s_{bd,e}^\sigma + s_{bu,e}^\sigma). \quad (56)$$

The leading term of  $s_{bu,e}^\sigma$  is the  $\tilde{Q}$  interaction term, which is proportional to  $(T/\mu_q)^{2/3}$  from Eq. (54) (third case), while the leading term of  $s_{bd,e}^\sigma$  is  $(T/\mu_q)$  from (54) (first and second cases). If we only keep the  $\tilde{Q}$  interaction term in  $s_{bu,e}^\sigma$ , then we have

$$\begin{aligned} \sigma_e &= \frac{\mu_e^2 (Q_e^{\tilde{Q}})^2}{\pi^2} \frac{4\pi^3}{3T s_{bu,e}^\sigma} \\ &= \frac{\mu_e^2 (Q_e^{\tilde{Q}})^2}{\pi^2} \frac{8\pi^2 \Lambda^{2/3}}{\Gamma(8/3)\zeta(5/3)T^{5/3} (Q_{bu}^{\tilde{Q}})^2 (Q_e^{\tilde{Q}})^2} \\ &\simeq \frac{\mu_q^2 e^2}{\pi^2} \frac{0.0433}{\alpha^{5/3} T (T/\mu_q)^{2/3}}, \end{aligned} \quad (57)$$

which agrees with the numerical result to 5% at  $T = 10^{-5}\mu_q$  and 22% at  $T = 10^{-3}\mu_q$ . We thus conclude that for the electrical conductivity of  $\tilde{Q}$  charge, the dominant contribution comes from the electron, and the relevant scattering process in leading order of  $T/\mu_q$  is between the electron and the blue up quark via the  $\tilde{Q}$  interaction.

#### D. Thermal conductivity

For the thermal conductivity, the discussion of Sec. IV A applies straightforwardly, as we now demonstrate. We have  $\phi_i = (\epsilon - \mu_i)v_\alpha$  and  $\gamma = 3$  in Eq. (44), which then gives

$$\kappa_i = \tau_i^\kappa \frac{\mu_i^2 T}{3}. \quad (58)$$

To calculate  $\kappa_i$  using Eq. (48) in the limit  $\omega \ll q$  and  $T \ll \mu_q$ , we write

$$\begin{aligned} &\phi_1 \cdot [\tau_i^\kappa (\psi_1 - \psi_3) + \tau_j^\kappa (\psi_2 - \psi_4)] \\ &= \frac{\phi_1 - \phi_3}{2T} \cdot [\tau_i^\kappa (\psi_1 - \psi_3) + \tau_j^\kappa (\psi_2 - \psi_4)] \\ &= \frac{\omega^2}{2T} \left[ \tau_i^\kappa + \frac{q^2}{4p_1 p_2} \tau_j^\kappa \right. \\ &\quad \left. - \cos\theta \sqrt{\left(1 - \frac{q^2}{4p_1^2}\right) \left(1 - \frac{q^2}{4p_2^2}\right)} \tau_j^\kappa \right]. \end{aligned} \quad (59)$$

Using the above two equations in Eq. (48), we have

$$1 = \frac{9}{4\pi^5 T} \sum_j \mu_j^2 (\tau_i^\kappa s_{ij} + \tau_j^\kappa \tilde{s}_{ij}), \quad (60)$$

for each flavor  $i$ , where

$$\begin{aligned} s_{ij}^\kappa &= \int_0^\infty d\omega \left( \frac{\omega/2T}{\sinh(\omega/2T)} \right)^2 \int_0^{q_m} dq \int_0^{2\pi} \frac{d\theta}{2\pi} |M_{ij}|^2 \omega^2, \\ \tilde{s}_{ij}^\kappa &= \int_0^\infty d\omega \left( \frac{\omega/2T}{\sinh(\omega/2T)} \right)^2 \int_0^{q_m} dq \int_0^{2\pi} \frac{d\theta}{2\pi} |M_{ij}|^2 \\ &\quad \times \omega^2 \left( \frac{q^2}{4p_1 p_2} - \cos\theta \sqrt{\left(1 - \frac{q^2}{4p_1^2}\right) \left(1 - \frac{q^2}{4p_2^2}\right)} \right), \end{aligned} \quad (61)$$

which are symmetric in exchanging  $i$  and  $j$ . We numerically evaluate both  $s_{ij}^\kappa$  and  $\tilde{s}_{ij}^\kappa$  as functions of  $T/\mu_q$  using the scattering matrix element  $M_{ij}$  given in Eq. (19), with the charges from Table I with  $\alpha = 1/137$  and  $\alpha_s = 1$ ,  $L$ 's from Eq. (20) with  $p_1 = \mu_i$  and  $p_2 = \mu_j$ , the boson self-energies from Eqs. (25)–(28), and the chemical potentials from Eq. (4). We then solve the three relaxation times from the three equations in Eq. (60), and we use  $\tau_i^\kappa \mu_q$  in Eq. (58) to obtain  $\kappa_i/\mu_q^2$ . The results are plotted in Fig. 2, and the best fits are  $\kappa_{bu}/\mu_q^2 = 5.69/(1 + 3720(T/\mu_q))$ ,  $\kappa_{bd}/\mu_q^2 = 0.00617/(T/\mu_q)$ , and  $\kappa_e/\mu_q^2 = 6.70/(1 + 6.92(T/\mu_q)^{2/3})$ . We note these fits can be extrapolated to arbitrary low temperature.

We see in Fig. 2 the expected gradual transition from a low-temperature regime dominated by blue down quarks to a high-temperature regime dominated by electrons. We now derive approximate analytic expressions to account for this behavior, by assuming that the momentum transfer  $q$  is much less than the typical Fermi momenta [12]. We use the identities,

$$\begin{aligned} &\int_0^\infty d\omega \left( \frac{\omega/2T}{\sinh(\omega/2T)} \right)^2 \int_0^\infty dq \operatorname{Re} \left[ \frac{\omega^2}{(q^2 + \Pi^{aa})(q^2 + \Pi^{bb})^*} \right] \\ &= \begin{cases} \frac{2\pi^5 T^3}{15(\Pi^{aa}\sqrt{\Pi^{bb} + \Pi^{bb}\sqrt{\Pi^{aa}}})} & \text{if neither } a \text{ nor } b \text{ is } \tilde{Q} \\ \frac{\pi\Gamma(14/3)\zeta(11/3)T^{8/3}}{3\Pi^{aa}\Lambda^{2/3}} - \frac{2\pi^5 T^3}{15(\Pi^{aa})^{3/2}} + \mathcal{O}\left(\frac{T^{10/3}}{\mu_q}\right) & \text{if } b \text{ is } \tilde{Q} \text{ and } a \text{ is not } \\ \frac{\pi\zeta(3)T^2}{\Lambda^2} & \text{if } a \text{ and } b \text{ are both } \tilde{Q} \end{cases} \end{aligned} \quad (62)$$



For the second case, we keep up to  $T^3/\mu_q^3$ , which is the same order as the first case. This allows us to obtain a closed form for  $s^\kappa$  and  $\tilde{s}^\kappa$  up to  $T^3/\mu_q^3$ ,

$$s_{ij}^\kappa = \frac{\pi\zeta(3)T^2}{2} \frac{(Q_i^{\tilde{Q}})^2(Q_j^{\tilde{Q}})^2}{\Lambda^2} + \frac{\pi\Gamma(14/3)\zeta(11/3)T^{8/3}}{3} \frac{Q_i^X Q_j^X Q_i^{\tilde{Q}} Q_j^{\tilde{Q}}}{\Pi_i^{XX} \Lambda^{2/3}} + \frac{2\pi^5 T^3}{15} \left[ -\frac{Q_i^X Q_j^X Q_i^{\tilde{Q}} Q_j^{\tilde{Q}}}{(\Pi_i^{XX})^{3/2}} + \sum_{a,b=\{T_8,Q\}} \frac{Q_i^a Q_j^a Q_i^b Q_j^b}{\Pi_i^{aa} \sqrt{\Pi_i^{bb}} + \Pi_i^{bb} \sqrt{\Pi_i^{aa}}} + \frac{1}{2} \frac{(Q_i^X)^2 (Q_j^X)^2}{2 \Pi_i^{XX} \sqrt{\Pi_i^{XX}}} \right], \quad (63)$$

and

$$\tilde{s}_{ij}^\kappa = \frac{\pi\Gamma(14/3)\zeta(11/3)T^{8/3}}{3} \sum_{a=\{T_8,Q\}} \frac{Q_i^a Q_j^a Q_i^{\tilde{Q}} Q_j^{\tilde{Q}}}{\Pi_i^{aa} \Lambda^{2/3}} + \frac{2\pi^5 T^3}{15} \sum_{a=\{T_8,Q\}} \left[ -\frac{Q_i^a Q_j^a Q_i^{\tilde{Q}} Q_j^{\tilde{Q}}}{(\Pi_i^{aa})^{3/2}} + \frac{Q_i^a Q_j^a Q_i^X Q_j^X}{\Pi_i^{aa} \sqrt{\Pi_i^{XX}} + \Pi_i^{XX} \sqrt{\Pi_i^{aa}}} \right]. \quad (64)$$

The term proportional to  $T^2$  in  $s^\kappa$  comes from the  $\tilde{Q}$  interaction, while the terms proportional to  $T^3$  in  $s^\kappa$  and  $\tilde{s}^\kappa$  come from the screened interactions by the  $Q$ ,  $T_8$ , and  $X$  bosons. The term proportional to  $T^{8/3}$  is the cross term of the  $\tilde{Q}$  interaction and screened interactions in the scattering matrix  $|M_{ij}|^2$ . As shown in [12], the  $\tilde{Q}$ -interaction term has a lower power of temperature because of the Landau damping, and it is the leading term at lower temperature. Using these expressions in Eq. (60), we can solve for the  $\tau_i^\kappa$  in closed form. These expressions are, however, lengthy, so we only show results for  $\alpha_s = 1$  and  $\alpha = 1/137$ , expanding  $1/\tau_i^\kappa$  to order of  $T/\mu_q$  to obtain

$$\kappa_{bu} \simeq \frac{\mu_q^2}{3} \frac{16.9}{1 + 75.3(T/\mu_q)^{2/3} + 3350(T/\mu_q)}, \quad (65)$$

$$\kappa_{bd} \simeq \frac{\mu_q^2}{3} \frac{0.0189}{T/\mu_q}, \quad (66)$$

$$\kappa_e \simeq \frac{\mu_q^2}{3} \frac{20.0}{1 + 29.9(T/\mu_q)^{2/3} - 58.8(T/\mu_q)}, \quad (67)$$

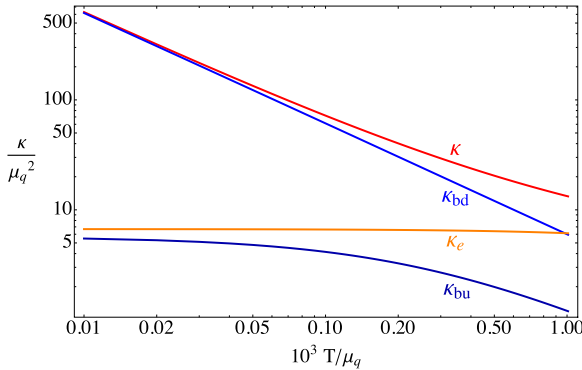


FIG. 2. (Color online) Numerically calculated thermal conductivity in units of quark chemical potential  $\mu_q$  in the 2SC phase with  $\alpha_s = 1$ . In this temperature range we see the crossover from electron domination at high temperature to blue down quark domination at low temperature (see Sec. IV A).

which agree with the numerical results to within 11% for  $\kappa_{bu}$ , 6% for  $\kappa_{bd}$ , and 12% for  $\kappa_e$  at temperatures up to  $10^{-3}\mu_q$ . In the denominators of the expressions above for  $\kappa_i$ , we see terms proportional to  $T^0$ ,  $T^{2/3}$ , and  $T$ . The terms of order  $T^0$  arise from electromagnetic scattering of the relevant fermion by the background of charged gapless fermions. This interaction is mediated by  $\tilde{Q}$  photons, and the power of  $T$  is determined by the Landau damping of the transverse  $\tilde{Q}$  photon propagator as shown in Eq. (28). The terms of order  $T^{2/3}$  arise from the cross term of  $\tilde{Q}$  and screened interactions in  $s^\kappa$  and  $\tilde{s}^\kappa$ , and the terms of order  $T$  arise from the screened interactions in  $s^\kappa$  and  $\tilde{s}^\kappa$ . We can now use these physical insights to obtain analytic expressions for some of the numerical coefficients in (65)–(67).

If we take the  $\tilde{Q}$ -interaction term and ignore the other terms in  $s^\kappa$  and  $\tilde{s}^\kappa$ , then we can solve Eq. (60) for  $\tau_{bu}^\kappa$  and  $\tau_e^\kappa$  exactly. For  $\kappa_e$ , from Eq. (58), we have

$$\kappa_e = \frac{\mu_e^2 T}{3} \frac{4\pi^5 T}{9\mu_e^2 (s_{e,e}^\kappa + s_{e,bu}^\kappa)} = \frac{4\pi^4}{27\zeta(3)} \frac{\Lambda^2}{(Q_e^{\tilde{Q}})^4} \simeq \frac{\mu_q^2}{3} \frac{0.146}{\alpha}, \quad (68)$$

which gives the leading  $T^0$  term in Eq. (67). For  $\kappa_{bu}$ , the same approximation yields an expression similar to Eq. (68), but this is not a good approximation at  $T/\mu_q \simeq 10^{-3}$  because the coefficients of the higher-order terms of  $T/\mu_q$  are large as we can see in Eq. (65). This is because they arise from the strong interaction. For  $\kappa_{bd}$ , the leading order for the denominator is  $T$ , which comes from the screened  $T^8$ ,  $X$ , and  $Q$  interactions, but we can ignore the  $Q$  interaction because  $e/g$  is small. The analytic solution then becomes

$$\kappa_{bd} = \frac{\mu_{bd}^2 T}{3} \frac{16\pi^5 T}{9\mu_{bd}^2 (s_{bu,bd}^\kappa + 4s_{bd,bd}^\kappa + 4\tilde{s}_{bd,bd}^\kappa)}, \quad (69)$$

with

$$s_{bu,bd}^\kappa + 4s_{bd,bd}^\kappa + 4\tilde{s}_{bd,bd}^\kappa = \frac{2\pi^5 T^3}{15} \left[ \frac{(Q_{bu}^{T_8})^2 (Q_{bd}^{T_8})^2 + 4(Q_{bd}^{T_8})^4}{2(\Pi_i^{T_8 T_8})^{3/2}} \right]$$

$$+ \left. \begin{aligned} & \frac{(Q_{bu}^X)^2(Q_{bd}^X)^2 + 4(Q_{bd}^X)^4}{4(\Pi_i^{XX})^{3/2}} \\ & + \frac{4(Q_{bd}^{T_8})^2(Q_{bd}^X)^2}{\Pi_i^{T_8 T_8} \sqrt{\Pi_i^{XX}} + \Pi_i^{XX} \sqrt{\Pi_i^{T_8 T_8}}} \end{aligned} \right],$$

which gives Eq. (66). Therefore, the relevant scattering process in leading order of  $T/\mu_q$  for  $\kappa_e$  is between electrons and blue up quarks via the  $\tilde{Q}$  interaction, and the relevant scattering process in leading order of  $T/\mu_q$  for  $\kappa_{bd}$  is between  $bd$  and  $bu$  quarks via the strong interactions.

The approximate temperature when  $\kappa_{bd}$  crosses  $\kappa_e$  can be calculated from Eqs. (68) and (69):

$$\frac{\kappa_e}{\kappa_{bd}} = \frac{s_{bu,bd}^\kappa/4 + s_{bd,bd}^\kappa + \tilde{s}_{bd,bd}^\kappa}{s_{e,e}^\kappa + s_{e,bu}^\kappa} \simeq 7.73 \frac{\alpha_s^{1/2}(T/\mu_q)^3}{\alpha(T/\mu_q)^2}, \quad (70)$$

which crosses unity at  $T/\mu_q \simeq \alpha/(7.73\alpha_s^{1/2}) \simeq 10^{-3}$ . The factor of 7.73 is a numerical constant whose only physics content is the charges of the fermions; it is independent of  $e, g, \mu_q$ , and  $T$ . As we anticipated, the thermal conductivity is dominated by blue down quarks at lower temperature because they do not have  $\tilde{Q}$  charge and so do not feel the long-ranged (Landau-damped)  $\tilde{Q}$  interaction. Their relaxation time is determined by the screened strong interactions, so the total thermal conductivity in the 2SC phase goes as  $1/T$ . This behavior is different from unpaired quark matter, in which the thermal conductivity has a constant value in the low temperature limit because of the unscreened magnetic gluon interaction (see Sec. VI).

### E. Shear viscosity

For the shear viscosity, the transition described in Sec. IV A occurs only at very low temperature, so, as we now demonstrate, electrons dominate in most of the temperature range we study. We have  $\phi = p_\alpha v_\beta$  and  $\gamma = 5$  in Eq. (44), which then gives

$$\eta_i = \tau_i^\eta \frac{\mu_i^4}{5\pi^2}, \quad (71)$$

where  $\tau_i^\eta$  is the relaxation time for the fermion flavor  $i$ . To calculate  $\eta_i$  using Eq. (48) in the limit  $\omega \ll q$  and  $T \ll \mu_q$ , we write

$$\begin{aligned} & \phi_1 \cdot [\tau_i^\eta(\psi_1 - \psi_3) + \tau_j^\eta(\psi_2 - \psi_4)] \\ & = \frac{q^2}{2} \left(1 - \frac{q^2}{4p_1^2}\right) \tau_i^\eta \\ & \quad - \frac{q^2}{2} \cos\theta \sqrt{\left(1 - \frac{q^2}{4p_1^2}\right)\left(1 - \frac{q^2}{4p_2^2}\right)} \tau_j^\eta. \end{aligned} \quad (72)$$

Using these two equations in Eq. (48), we have

$$1 = \frac{9T}{4\pi^3} \sum_j \frac{\mu_j^2}{\mu_i^2} (\tau_i^\eta s_{ij}^\eta + \tau_j^\eta \tilde{s}_{ij}^\eta), \quad (73)$$

for each flavor  $i$ , where

$$\begin{aligned} s_{ij}^\eta &= \int_0^\infty d\omega \left( \frac{\omega/2T}{\sinh(\omega/2T)} \right)^2 \int_0^{q_M} dq \\ & \quad \times \int_0^{2\pi} \frac{d\theta}{2\pi} |M_{ij}|^2 q^2 \left(1 - \frac{q^2}{4p_1^2}\right), \\ \tilde{s}_{ij}^\eta &= - \int_0^\infty d\omega \left( \frac{\omega/2T}{\sinh(\omega/2T)} \right)^2 \int_0^{q_M} dq \int_0^{2\pi} \frac{d\theta}{2\pi} |M_{ij}|^2 q^2 \\ & \quad \times \cos\theta \sqrt{\left(1 - \frac{q^2}{4p_1^2}\right)\left(1 - \frac{q^2}{4p_2^2}\right)}, \end{aligned} \quad (74)$$

which are both symmetric in exchanging  $i$  and  $j$ . We numerically evaluate both  $s_{ij}^\eta$  and  $\tilde{s}_{ij}^\eta$  as functions of  $T/\mu_q$  using the same parameters used in the case of the electrical conductivity. We then solve for the three relaxation times from the three equations in Eq. (73), and we use  $\tau_i^\eta \mu_q$  in Eq. (71) to obtain  $\eta_i/\mu_q^3$ . In Fig. 3 we show the temperature dependence of the shear viscosity, and the best fits are  $\eta_{bu}/\mu_q^3 = 0.150/(T/\mu_q)^{5/3} + 2490(T/\mu_q)^2$ ,  $\eta_{bd}/\mu_q^3 = 0.00443/(T/\mu_q)^2$ , and  $\eta_e/\mu_q^3 = 0.171/(T/\mu_q)^{5/3} + 2.78(T/\mu_q)^2$ . We note these fits can be extrapolated to arbitrary low temperature. We can see that the electrons dominate in most of the temperature range we study, but there is a transition to the  $bd$ -dominated regime at low temperature,  $T \simeq 2.2 \times 10^{-5} \mu_q$ . In the temperature range of Fig. 3, the blue up contribution to the total shear viscosity is less than 0.8%.

We now derive approximate analytic expressions by assuming that the momentum transfer is much less than the Fermi momenta ( $q \ll \mu_q$ ). Then, as for the electrical conductivity, we can obtain a closed form for  $s^\eta$  and  $\tilde{s}^\eta$  using Eq. (54). In this limit, we have  $s_{ij}^\eta = s_{ij}^\sigma$  in Eq. (55) and

$$\tilde{s}_{ij}^\eta = \frac{\pi^3 T}{6} \sum_{a=\{T_8, Q\}} \left[ \frac{Q_i^a Q_j^a Q_i^X Q_j^X}{\sqrt{\Pi_i^{aa}} + \sqrt{\Pi_i^{XX}}} + \frac{Q_i^a Q_j^a Q_i^{\tilde{Q}} Q_j^{\tilde{Q}}}{\sqrt{\Pi_i^{aa}}} \right]. \quad (75)$$

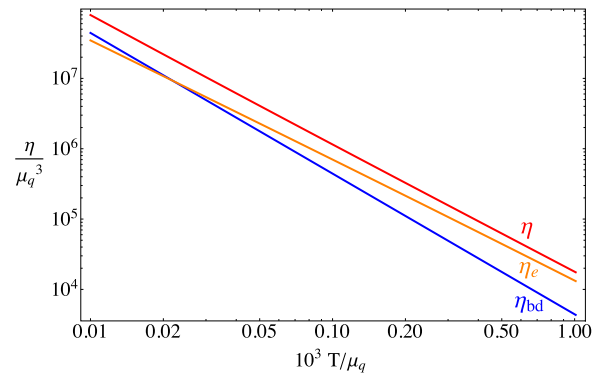


FIG. 3. (Color online) Numerical calculation of shear viscosity as a function of temperature, taking  $\alpha_s = 1$ . In this temperature range we see the crossover from electron domination at high temperature to blue down quark domination at low temperature (see Sec. IV A).

Using  $s_{ij}^\eta$  and  $\tilde{s}_{ij}^\eta$  in Eq. (73), we can solve the three relaxation times in closed form. These expressions are lengthy, so we only show results for  $\alpha_s = 1$  and  $\alpha = 1/137$ , expanding  $1/\tau_i^\eta$  to order of  $T(T/\mu_q)$  to obtain

$$\eta_{bd} \simeq \frac{\mu_q^4}{5\pi^2} \frac{0.111}{T(T/\mu_q)}, \quad (76)$$

$$\eta_e \simeq \frac{\mu_q^4}{5\pi^2} \frac{8.42}{T(T/\mu_q)^{2/3} + 5.56T(T/\mu_q)}, \quad (77)$$

which agree with the numerical calculations to within 50% for  $\eta_{bd}$  and 18% for  $\eta_e$  at temperatures up to  $10^{-3}\mu_q$ . As pointed out by Heiselberg and Pethick [12], the shear viscosity and the electrical conductivity vary as a different power of temperature from the thermal conductivity, because they are weighted by the momentum transfer rather than the energy transfer. Consequently, the ratio  $\eta_{bd}/\eta_e$  becomes of order 1 at  $T/\mu_q \sim 10^{-5}$  instead of  $10^{-3}$  (70), so most of our temperature range (shown in Fig. 3) is in the ‘‘high temperature’’ regime of Sec. IV A.

We write down the analytic forms of the leading terms of  $\eta_e$  and  $\eta_{bd}$  and identify the relevant scattering processes. For  $\eta_e$ , we can obtain the leading order of  $T$  by performing an analytic calculation of the  $\tilde{Q}$  interactions alone. The solution of Eq. (73) can then be simplified and becomes

$$\begin{aligned} \eta_e &= \frac{\mu_e^4}{5\pi^2} \frac{4\pi^3}{9T(s_{e,e}^\eta + s_{e,bu}^\eta)} \\ &= \frac{\mu_e^4}{5\pi^2} \frac{8\pi^2 \Lambda^{2/3}}{3\Gamma(8/3)\zeta(5/3)T^{5/3}((Q_e^{\tilde{Q}})^4 + (Q_e^{\tilde{Q}})^2(Q_{bu}^{\tilde{Q}})^2)} \\ &\simeq \frac{\mu_q^4}{5\pi^2} \frac{0.00231}{\alpha^{5/3}T(T/\mu_q)^{2/3}}, \end{aligned} \quad (78)$$

which is Eq. (77) without the second term. This agrees with the numerically calculated expression to 5% at  $T = 10^{-5}\mu_q$  and 30% at  $T = 10^{-3}\mu_q$ . For  $\eta_{bd}$  the relaxation time is determined by the screened  $T^8$ ,  $X$ , and  $Q$  interactions, but we can ignore the  $Q$  interaction because  $e/g$  is small. The analytic solution then becomes

$$\eta_{bd} = \frac{\mu_{bd}^4}{5\pi^2} \frac{16\pi^3}{9T(s_{bu,bd}^\eta + 4s_{bd,bd}^\eta + 4\tilde{s}_{bd,bd}^\eta)}, \quad (79)$$

with

$$\begin{aligned} &s_{bu,bd}^\eta + 4s_{bd,bd}^\eta + 4\tilde{s}_{bd,bd}^\eta \\ &= \frac{\pi^3 T}{6} \left[ \frac{(Q_{bu}^{T_8})^2 (Q_{bd}^{T_8})^2 + 4(Q_{bd}^{T_8})^4}{2\sqrt{\Pi_l^{T_8 T_8}}} \right. \\ &\quad \left. + \frac{(Q_{bu}^X)^2 (Q_{bd}^X)^2 + 4(Q_{bd}^X)^4}{4\sqrt{\Pi_l^{XX}}} + \frac{4(Q_{bd}^{T_8})^2 (Q_{bd}^X)^2}{\sqrt{\Pi_l^{T_8 T_8}} + \sqrt{\Pi_l^{XX}}} \right], \end{aligned}$$

which gives Eq. (76). Therefore, as in the case of the thermal conductivity, the relevant scattering process in leading order of  $T/\mu_q$  for  $\eta_e$  is between electrons and blue up quarks via the  $\tilde{Q}$  interaction, and the relevant scattering process in leading

order of  $T/\mu_q$  for  $\eta_{bd}$  is between  $bd$  and  $bu$  quarks via the strong interactions.

The approximate temperature when  $\eta_{bd}$  becomes equal to  $\eta_e$  can be calculated from Eqs. (78) and (79),

$$\begin{aligned} \frac{\eta_e}{\eta_{bd}} &= \frac{\mu_e^4 s_{bu,bd}^\eta/4 + s_{bd,bd}^\eta + \tilde{s}_{bd,bd}^\eta}{\mu_{bd}^4 (s_{e,e}^\eta + s_{e,bu}^\eta)} \\ &\simeq \frac{0.331}{2^4} \frac{\alpha_s^{3/2}(T/\mu_q)}{\alpha^{5/3}(T/\mu_q)^{2/3}}, \end{aligned} \quad (80)$$

which crosses unity when  $T/\mu_q \simeq (2^4 \alpha^{5/3})^3 / (0.331 \alpha_s^{3/2})^3 \sim 10^{-5}$ . The factor of 0.331 is a numerical constant whose only physics content is the charges of the fermions; it is independent of  $e, g, \mu_q$ , and  $T$ . As noted above, this crossover temperature is much lower than that for the thermal conductivity given in Eq. (70). The reason is as follows. As we reduce the temperature, the crossover occurs when the  $\tilde{Q}$  interaction becomes long ranged, so the electron mean free path becomes short, suppressing the electron contribution to transport relative to that of the  $\tilde{Q}$ -neutral  $bd$  quarks (see Sec. IV A). However, shear viscosity and thermal conductivity have different sensitivity to the increase in the range of the  $\tilde{Q}$  interaction. For shear viscosity the relevant collisions are those that transfer higher momentum [this is related to the weight of  $q^2$  in (74)], so the increase in the range of the  $\tilde{Q}$  interaction only has a modest impact on the mean free path because the long-range interactions involve low momentum transfer, and do not contribute much to shear viscosity. For thermal conductivity, the relevant collisions are those that transfer energy (of order  $T$  typically), hence the weight of  $\omega^2$  in (61), and even the low momentum transfer interactions are able to do this. This means that as we reduce the temperature, increasing the range of the  $\tilde{Q}$  interaction, the contribution to shear viscosity from electrons is only moderately suppressed relative to that from  $bd$  quarks, whereas the contribution to thermal conductivity from electrons is heavily suppressed relative to that from  $bd$  quarks. Consequently, for shear viscosity we have to go to much lower temperatures to reduce the electron contribution to the same level as the  $bd$  contribution.

## V. VORTEX-FERMION SCATTERING CONTRIBUTION TO THE TRANSPORT

If the 2SC core of a neutron star forms in the presence of a magnetic field, it will be penetrated by the  $\tilde{Q}$  component of the field, but behave as a type-II superconductor with respect to the  $X$  component, so the  $X$  flux is concentrated into ‘‘color-magnetic’’ flux tubes [16]. It is not yet clear whether these flux tubes are energetically stable, but in this section we estimate their possible contribution to the transport via scattering of ungapped fermions off the flux tubes. Because the density of flux tubes is independent of temperature, but the density of ungapped fermions decreases with  $T$ , flux-tube scattering will eventually dominate the transport at sufficiently low temperatures.

For a given transport coefficient  $\xi = \{\sigma, \kappa, \eta\}$  the relaxation time  $\tau_i^\xi$  of a fermion of type  $i$  is inversely proportional to

the sum of the inverse relaxation times associated with the different scattering channels:

$$\frac{1}{\tau_i^\xi} = \frac{1}{\tau_{i,v}^\xi} + \sum_j \frac{1}{\tau_{ij}^\xi}, \quad (81)$$

where  $1/\tau_{i,v}^\xi$  and  $1/\tau_{ij}^\xi$  are the fermion-vortex and fermion-fermion relaxation rates, respectively. To give a simple estimate, we assume that the fermion-vortex and fermion-fermion relaxation rates are decoupled, so  $\sum_j 1/\tau_{ij}^\xi$  is simply the inverse of the relaxation times which we have computed in the previous section. It is then clear from this expression that the fermion-vortex scattering process only increases the total relaxation rate and thus only suppresses the transport coefficient.

The vortex-fermion contribution was discussed in [16], and here we give a brief explanation of the result. The  $X$ -flux tubes have area density  $n_v = B/\Phi_X$ , where  $\Phi_X = 6\pi/e$ . The ungapped fermions will scatter off the color-magnetic flux tubes via the Aharonov-Bohm effect. The cross section of the Aharonov-Bohm scattering is proportional to  $\sin^2(\pi\tilde{\beta}_i)/\mu_i$ , where  $\tilde{\beta}_i$  is a measure of the Aharonov-Bohm interaction of the fermion of type  $i$  with the  $X$ -flux tube. The  $bu$  quark and the electron have the same factor  $\sin^2(\pi\tilde{\beta}_i) \simeq \pi^2\alpha^2/\alpha_s^2$ , while for the  $bd$  quark this factor is zero [16]. Because the vortex does not interact with the blue down quark, it does not affect the blue down quark contributions to the transport coefficients.

*Thermal conductivity.* From the previous section, we have found that the dominant contribution to the thermal conductivity is from blue down quarks, which do not interact with vortices. Therefore, the vortex scattering process only suppresses the subdominant contributions and does not affect the total thermal conductivity in the temperature range we have considered in the previous section.

*Electrical conductivity and shear viscosity.* In the absence of vortices, we have found in the previous section that the dominant contribution to both the electrical conductivity and the shear viscosity is from electrons, and the most relevant interaction for the relaxation rate is the  $\tilde{Q}$  interaction. From Eqs. (49) and (57) for the electrical conductivity and from Eqs. (71) and (78) for the shear viscosity, we can read off the relaxation rates of the electron for the two transport coefficients and write them as

$$\sum_j \frac{1}{\tau_{e,j}^\xi} = c_\xi \alpha^{5/3} \frac{T^{5/3}}{\mu_q^{2/3}}, \quad (82)$$

where  $\xi = \{\sigma, \eta\}$  and for each  $\xi$ ,  $c_\xi$  is a numerical constant of order 10, which depends on the charges of the fermions. According to [16], the momentum relaxation rate for the electron-vortex scattering is

$$\frac{1}{\tau_{e,v}} = \frac{\pi^{3/2} \alpha^{5/2} B}{3\alpha_s^2 \mu_e}. \quad (83)$$

We expect, as is the case for the fermion-fermion relaxation rates [12], that the electron-vortex relaxation rates for electrical conductivity and shear viscosity are the same as the momentum relaxation rate up to a constant of order 1. Electron-vortex scattering becomes important when its rate (83) becomes

comparable to the fermion-fermion relaxation rate (82). Taking  $\alpha_s = 1$  and assuming typical chemical potential  $\mu_q = 400$  MeV and the lowest possible temperature in neutron stars to be  $T = 10^7$  K, we find that the ratio of the rates becomes unity when the magnetic field reaches

$$B \sim 10^{12} \text{ G} \left( \frac{T}{10^7 \text{ K}} \right)^{5/3} \left( \frac{\mu_q}{400 \text{ MeV}} \right)^{1/3}. \quad (84)$$

From the above estimates, we conclude that the presence of the vortices in realistic values of the external magnetic field can lower the transport coefficients we have computed in the previous section. Therefore, performing more complete computations of transport coefficients with the presence of vortices may be necessary if the vortex in the 2SC phase turns out to be stable.

## VI. CONCLUSIONS

We have calculated the electrical conductivity, thermal conductivity, and shear viscosity of quark matter in the 2SC phase using the linearized Boltzmann equation in the relaxation time approximation. We have relied on perturbation theory and used the leading order in  $\alpha$  and  $\alpha_s$  for the scattering matrix element. For the numerical computations, we have assumed that the energy transfer  $\omega$  is much smaller than the momentum transfer  $q$  (the static limit) and have taken the leading order in  $\omega/q$ . In the temperature range  $10^{-5} < T/\mu_q < 10^{-3}$ , this approximation is good because the characteristic energy transfer is temperature, while the characteristic momentum transfer is the Debye screening mass. The results are shown in Figs. 1–3 for  $\alpha_s = 1$ . For physical insight, we have obtained approximate analytic results by further assuming that the momentum transfer is much smaller than the quark chemical potential,  $q \ll \mu_q$ . For the electrical (57) and thermal (69) conductivities, the analytic results of the leading fermion contributions agree with the numerical results of the leading fermion contributions to within 22% and 6%, respectively. For the shear viscosity, the leading (electron) contribution (77) agrees with the numerical result of the leading fermion contribution to within about 18% over the relevant temperature range.

The general picture of transport in the 2SC phase is that it occurs via the ungapped fermions, which are the blue up quark, the blue down quark, and the electron. The electron contribution dominates at higher temperature because electrons do not feel the strong interaction, only the electromagnetic interaction, and so have longer relaxation times than the ungapped quarks. However, at low temperature the  $\tilde{Q}$  interaction becomes long ranged because it is Landau damped (not Meissner screened), and this compensates for its small inherent coupling. The  $\tilde{Q}$ -neutral blue down quark therefore dominates transport at low temperatures, because its interactions, although strong, are screened.

*Thermal conductivity.* The crossover from blue-down to electron domination occurs at  $T/\mu_q \sim \alpha/7.7 \sim 10^{-3}$ , so most of the temperature range of interest for neutron stars is in the blue-down-dominated regime where  $\kappa \sim 1/T$ .

*Shear viscosity.* The crossover from blue-down to electron domination occurs at  $T/\mu_q \sim 10^{-5}$ , so electrons are dominant



down to  $T \sim 10$  keV. The crossover temperature for the shear viscosity is much smaller than for the thermal conductivity because the relevant collisions for shear viscosity are those that transfer higher momentum, so the increase in the range of the  $\tilde{Q}$  interaction has a smaller impact on the mean free path because the long-range interactions involve low momentum transfer. See the end of Sec. IV E.

*Electrical conductivity.* This is a special case because the transported quantity is  $\tilde{Q}$  charge, so the blue down quarks, which are  $\tilde{Q}$  neutral, do not contribute to the electrical conductivity. The electron contribution therefore dominates over the entire temperature range.

Other possible excitations that might contribute to the transport coefficients include the color-magnetic flux tubes and gluons in the unbroken gauge sector. Flux tubes are discussed in Sec. V, where we have argued that at sufficiently low temperature and high magnetic field, the vortex-fermion scattering via the Aharonov-Bohm effect may suppress the electron contributions to the electrical conductivity and shear viscosity.

We now argue that  $SU(2)_{rg}$  gluons do not contribute to the transport coefficients in 2SC quark matter. The glue sector of the unbroken  $SU(2)_{rg}$  gauge theory has a confinement scale  $\Lambda'_{QCD}$  which may be in the keV range, or as high as about 10 MeV and a coupling  $\alpha'_s \simeq (\pi\alpha_s/2)^{1/2}\Delta/\mu_q$  which is smaller than  $\alpha_s$  because of the partial screening of the Cooper pairs [7]. If  $T \ll \Lambda'_{QCD}$  then the gluons are confined into glue balls with mass of order  $\Lambda'_{QCD}$ , so their contributions to transport are exponentially suppressed. If  $T \gtrsim \Lambda'_{QCD}$  then the theory is deconfined, and the gluons can contribute to the transport coefficients. From dimensional analysis, we can estimate that the  $SU(2)$  gluon contributions to the thermal conductivity and the shear viscosity are  $\kappa_{\text{glue}} \sim T^2/\alpha_s'^2$  and  $\eta_{\text{glue}} \sim T^3/\alpha_s'^2$  where  $1/\alpha_s'^2$  comes from the scattering amplitude of the gluons. Comparing the gluon contributions with the blue down quark contributions for  $\alpha_s = 1$  [see Eqs. (69) and (79)], we have  $\kappa_{\text{glue}}/\kappa_{bd} \sim (T/\mu_q)^3(\mu_q/\Delta)^2$  and  $\eta_{\text{glue}}/\eta_{bd} \sim (T/\mu_q)^5(\mu_q/\Delta)^2$ , which are both much less than 1 because  $T/\mu_q \lesssim 10^{-3}$  and  $\mu_q/\Delta < 2\mu_q/\mu_e \lesssim 3.5$  for 2SC quark matter (see end of Sec. II A). The electrical conductivity has a contribution from the gluons because, like the blue up quark, they carry a  $\tilde{Q}$  charge arising from their color  $T_8$  charge. However, dimensional analysis shows that their contribution is  $\sigma_{\text{glue}} \sim e^2 T/\alpha_s'^2$ , which is also negligible compared to the electron contribution (57).

It is interesting to compare our results with the transport properties of two-flavor *unpaired* quark matter. Transport in unpaired quark matter is dominated by electrons and their electromagnetic scattering off gapless quarks. This is because there is no Meissner screening of the gluons; they are Landau damped like the photon, so both gluon and photon interactions become long ranged at low temperature, and there is no crossover to a regime where short-ranged strong interactions dominate transport. We therefore expect that the transport coefficients of unpaired two-flavor quark matter are similar to those we calculated as the electron contribution to 2SC quark matter [(57), (68), and (78)]. The electron contributions to the transport coefficients of unpaired quark matter can be easily computed. After performing calculations similar to those in Sec. II, we can show that the transverse component

of the photon self-energy and the electron chemical potential in unpaired quark matter are  $2.34i\omega\Lambda^2/q$  and  $0.219\mu_q$ , respectively. Note that the chemical potential of the electron in unpaired quark matter is smaller than in 2SC quark matter. Using these values in (57), (68), and (78), we find the electron contributions to the transport coefficient in unpaired quark matter are  $0.0070\sigma_e$ ,  $1.7\kappa_e$ , and  $0.022\eta_e$ . The electrical conductivity and shear viscosity are much smaller because of their  $\mu_e$  dependence. We conclude that the electrical conductivity and shear viscosity, which are dominated by electrons, have similar expressions in 2SC quark matter and unpaired two-flavor quark matter in the temperature range that we studied. However, the thermal conductivity of 2SC matter is dominated by  $bd$  quarks, and rises as  $\mu_q^3/T$  at low temperature, whereas in unpaired two-flavor quark matter it is dominated by electrons and tends to a constant value of order  $\mu_q^2$ . It is an interesting future project to compute the transport properties of unpaired quark matter numerically and give more rigorous comparison with 2SC quark matter.

One natural generalization of our results would be to analyze the 2+1 flavor case, where strange quarks help to ensure neutrality, and  $\mu_e$  is much smaller and depends on the strange quark mass. This will affect the dominance of electrons. Another application would be a more careful treatment of two-flavor and two-plus-one-flavor unpaired quark matter (to our knowledge, only three-flavor unpaired quark matter was treated in the literature [12] and it is a special case because of the absence of electrons). One could then go on to study applications of these results to the observables on neutron stars. Shear viscosity plays an important role in the spin-down behavior of neutron stars because it is one of the dissipation mechanisms that damps “r modes.” Without sufficient damping, r modes would arise spontaneously in fast-spinning neutron stars, spinning them down via emission of gravitational radiation [31,32]. Thermal conductivity is the key microscopic quantity that controls macroscopic thermal transport and equilibration in the dense cores of young (less than a few hundred years old) isolated neutron stars and in accreting transient x-ray sources. Hybrid compact stars with 2SC matter may relax thermally on time scales that are different from those of their hadronic counterparts and this can be tested observationally. Finally, electrical conductivity of 2SC matter determines the time scale for the decay of the component of magnetic field which is not frozen in the color-magnetic flux tubes. Addressing this problem requires (in addition to conductivities of various phases) knowledge of the large-scale structure of the magnetic field and, therefore, the current distribution within the star. The putative decay of the magnetic fields can be tested, for example, with the models of secular evolution of pulsars in the  $p$ - $\dot{p}$  diagram.

## ACKNOWLEDGMENTS

We thank Toru Kojo, Dirk Rischke, Andreas Schmitt, and Kai Schwenzer for useful discussions. This research was supported in part by the Offices of Nuclear Physics and High Energy Physics of the U.S. Department of Energy under Contracts No. DE-FG02-91ER40628 and No.



DE-FG02-05ER41375, the Sofja Kovalevskaja program of the Alexander von Humboldt Foundation, the Bielefeld Young

Researcher's Fund, and the Deutsche Forschungsgemeinschaft (Grant No. SE 1836/3-1).

- 
- [1] D. Bailin and A. Love, *Phys. Rept.* **107**, 325 (1984).  
[2] M. G. Alford, A. Schmitt, K. Rajagopal, and T. Schafer, *Rev. Mod. Phys.* **80**, 1455 (2008).  
[3] M. Alford, K. Rajagopal, and F. Wilczek, *Nucl. Phys. B* **537**, 443 (1999).  
[4] I. A. Shovkovy and P. J. Ellis, *Phys. Rev. C* **66**, 015802 (2002).  
[5] C. Manuel and F. J. Llanes-Estrada, *JCAP* **08** (2007) 001.  
[6] C. Manuel, A. Dobado, and F. J. Llanes-Estrada, *Journal of High Energy Physics* **09** (2005) 076 .  
[7] D. H. Rischke, D. T. Son, and M. A. Stephanov, *Phys. Rev. Lett.* **87**, 062001 (2001).  
[8] M. G. Alford, K. Rajagopal, and F. Wilczek, *Phys. Lett. B* **422**, 247 (1998).  
[9] M. G. Alford, J. Berges, and K. Rajagopal, *Nucl. Phys. B* **571**, 269 (2000).  
[10] K. Rajagopal and F. Wilczek, *Phys. Rev. Lett.* **86**, 3492 (2001).  
[11] I. Shovkovy and M. Huang, *Phys. Lett. B* **564**, 205 (2003).  
[12] H. Heiselberg and C. J. Pethick, *Phys. Rev. D* **48**, 2916 (1993).  
[13] H. A. Weldon, *Phys. Rev. D* **26**, 1394 (1982).  
[14] D. H. Rischke, *Prog. Part. Nucl. Phys.* **52**, 197 (2004).  
[15] A. Schmitt, Q. Wang, and D. H. Rischke, *Phys. Rev. D* **69**, 094017 (2004).  
[16] M. G. Alford and A. Sedrakian, *J. Phys. G* **37**, 075202 (2010).  
[17] P. Shternin and D. Yakovlev, *Phys. Rev. D* **78**, 063006 (2008).  
[18] M. G. Alford and G. Good, *Phys. Rev. C* **82**, 055805 (2010).  
[19] M. Alford and Q.-h. Wang, *J. Phys. G* **31**, 719 (2005).  
[20] D. H. Rischke, *Phys. Rev. D* **62**, 034007 (2000).  
[21] D. H. Rischke, *Phys. Rev. D* **64**, 094003 (2001).  
[22] D. H. Rischke and I. A. Shovkovy, *Phys. Rev. D* **66**, 054019 (2002).  
[23] L. D. Landau and E. M. Lifshitz, *Fluid Mechanics*, 2nd ed. (Pergamon, Oxford, 1987).  
[24] E. M. Lifshitz and L. P. Pitaevskii, *Physical Kinetics*, 1st ed. (Pergamon, Oxford, 1981).  
[25] E. Flowers and N. Itoh, *Astrophys. J.* **206**, 218 (1976).  
[26] E. Flowers and N. Itoh, *Astrophys. J.* **230**, 847 (1979).  
[27] K. Itakura, O. Morimatsu, and H. Otomo, *Phys. Rev. D* **77**, 014014 (2008).  
[28] P. Shternin and D. Yakovlev, *Phys. Rev. D* **75**, 103004 (2007).  
[29] G. Rupak and T. Schafer, *Phys. Rev. A* **76**, 053607 (2007).  
[30] M. G. Alford, M. Braby, and S. Mahmoodifar, *Phys. Rev. C* **81**, 025202 (2010).  
[31] M. G. Alford, S. Mahmoodifar, and K. Schwenzer, *Phys. Rev. D* **85**, 024007 (2012).  
[32] N. Andersson, K. Kokkotas, and B. F. Schutz, *Astrophys. J.* **510**, 846 (1999).